Environmental Contours based on Inverse SORM

Wei Chai[a]*, Bernt J. Leira[a]

[a]*Department of Marine Technology, Norwegian University of Science and Technology, Trondheim, Norway*

*corresponding author: chai.wei@ntnu.no

Abstract: It is well known that the full long-term response analysis is recognized as the most accurate and reliable method for evaluation of the extreme response in the design of ships and marine structures. However, such a method is time consuming for large and complex systems. To improve efficiency, the environmental contour method (ECM) is frequently used to approximate the long-term extreme response. The ECM is based on an environmental contour, which is traditionally obtained by the inverse first order reliability method (IFORM) with the assumption that the failure surface in the U space is approximated as a tangent plane at the design point. However, such an approximation underestimates the true failure probability if the failure surface in the U space is a concave set, and then the corresponding environmental contour would not be conservative for possible designs. In this work, a more conservative ISORM (inverse second order reliability method) contour is proposed. In this method, a specific second-order surface is applied to approximate the failure surface at the design point, and then the failure domain in the U space would always be overestimated since the corresponding safe domain is approximated and underestimated as a sphere, regardless of the shapes of the failure surfaces. Therefore, the generated environmental contour can be always conservative for design purposes. The differences of the environmental contours generated by different methods, i.e., the traditional IFORM and the proposed ISORM, are illustrated by relevant examples, such as the wave statistics, wind wave statistics, and first-year ice ridge statistics.

Keywords: environmental contours; IFORM; ISORM; ships and marine structures

1. Introduction

For marine structures subjected to environmental loads, such as wind, wave, ice forces, evaluation of the extreme response and the associated stresses or strains over its specific lifetime is necessary and important at the design stage [1]. Basically, a full long-term response analysis that accounts for the structural response from each short-term environmental condition and the

occurrence rate of each short-term condition is recognized as the most appropriate and accurate approach [2, 3]. However, such a long-term analysis is usually time-consuming and not efficient, especially for large and complex structures. In order to improve the computational efficiency, it can be simplified by either reducing the computation cost of each short-term analysis [4, 5] or developing approximate methods that require a lower number of short-term analyses, such as identification of the critical environmental conditions by linear analyses [6], the environmental contour method (ECM) [7].

The ECM is based on the environmental contour defined in the environmental parameter space, i.e., a collection of environmental parameters corresponding to a given return period. In this method, the desired long-term extreme response can be approximately estimated on the basis of the critical short-term conditions on the environment contour associated with the same return period [3, 8]. The environment contour is identified based on relevant probability distributions of the environmental parameters and is given as the forms of contour line (two environmental parameters), contour surface (three parameters) or contour manifolds (more than three parameters). After this work, short-term response analyses are performed only for a few conditions on the environmental contour and then the highest short-term response is identified for application. Finally, a fractile higher than the median level is applied to the largest short-term response statistics in order to approximate the long-term extreme response. The ECM offers a simplified and fast way to estimate the long-term extreme responses, and therefore, it has been widely used for the design of ships and marine structures, such as offshore platforms in waves [9, 10] and ice conditions [11], wave energy converters [12], wind turbine [13, 14], flexible risers [15].

It is seen that the environmental contour with a given return period plays a fundamental role for application of the ECM. The traditional approach to establishing the environmental contour is based on the inverse first order reliability method (IFORM) and the conditional modeling approach for the environmental parameters [8]. By this method, the environmental variables are transformed into independent standard normal variables via the Rosenblatt transformation, and then, a sphere with the desired radius is identified in the U space. Subsequently, the environmental contour for a given return period is obtained by re-transforming the sphere back to the original physical space (i.e., the inverse Rosenblatt transformation). Furthermore, in order to avoid the Rosenblatt transformation, which requires the joint distribution of the environmental variables described by a set of conditional distributions, the environmental contours can also be generated by the Nataf transformation [16], Monte Carlo simulations [17]

and the principal component analysis [18], etc.

The environmental contour for a given return period based on the IFORM implies that the contour is defined closely related to the first order reliability method (FORM) approximation. For the FORM, for estimating the failure probability of the system, the failure boundary is replaced with a tangent plane at the design point in the U space. It is known that when the true failure surface in the U space is a convex set, the FORM approximation gives an upper boundary to the true failure probability [17]. On the other hand, this approximation does underestimate the true failure probability if the failure surface in the U space is a concave set. Therefore, the generated environmental contour would not be conservative for design purpose. In order to avoid such a deficiency in the traditional IFORM-contour, different definitions of the environmental contours have been proposed, such as the alternative environmental contours based on direct Monte Carlo simulations [17, 19], the highest density contour (HDC) [20], the equi-shape contour [2].

In this work, the equi-shape contour is studied in detail. For development of this contour, the failure boundary of the system in the U space is approximated by a sphere with a radius equal to the distance between the origin point and the design point, and then the safe domain is approximated as the region covered by the sphere. By this method, the true failure probability will always be overestimated regardless of the shape of the failure surface since the real safe domain is always larger than the proposed sphere. Subsequently and inversely, for a given return period, the resulting environmental contours based on the sphere approximation could be always conservative for possible designs [2]. Because the safe domain is approximated as a sphere located at the origin point in the U space, the environmental contour is referred to as an equi-shape contour. Furthermore, the sphere approximation of the safe domain for the system is a type of the second order reliability method (SORM), and therefore, the developed environmental contour can also be referred to as the ISORM-contour.

In this paper, the principles of the environmental contours obtained by the traditional IFORM and the more conservative ISORM are presented. The differences of the environmental contours generated by different methods are illustrated by relevant examples, such as the wave statistics (two environmental variables), wind wave statistics (three variables) and the first-year ice ridge statistics used for the design of ice-capable ships (three variables). The ISORM-contour proposed in this work and its application for possible designs could provide valuable supplements to the current ECM, which is widely used for estimating the extreme responses of ships and marine structures.

2. FORM and IFORM for structural reliability analysis

In this section, the derivation of the full long-term extreme response and the approximate manners based on the FORM and IFORM for the long-term analysis are presented. To begin with, assume that each short-term environmental condition has a duration of τ-hours and the related short-term responses can be described by stationary processes [1, 3]. The environmental variables are defined as an n-dimensional vector $\boldsymbol{S} = (S_1, S_2, \ldots, S_n)^{\mathrm{T}}$ with the joint probability density function (PDF), $f_S(\boldsymbol{s})$.

Assume that $\tilde{Y}$ denotes the short-term extreme response during a specific short-term condition $\boldsymbol{s}$, and then the corresponding cumulative density function (CDF) for the short-term extreme response is represented as $F_{\tilde{Y}|\mathbf{S}}$. Let the variable Y represent the long-term extreme response by considering the contribution from each short-term environmental condition. By applying the all short-term extremes method [1], the long-term CDF of the short-term extreme response can be approximated as:

$$F_Y(y) = \int_{R^n} F_{\tilde{Y}|\mathbf{S}}(y|\mathbf{s}) f_{\mathbf{S}}(\mathbf{s}) d\mathbf{s} \tag{1}$$

However, it is found that Eq. (1) is not an ergodic average, and the long-term distribution of the short-term extreme response should be modified as [21]:

$$F_Y(y) = \exp\left\{\int_{R^n} \ln\left[F_{\tilde{Y}|\mathbf{S}}(y|\mathbf{s})\right] f_{\mathbf{S}}(\mathbf{s}) d\mathbf{s}\right\} \tag{2}$$

In addition to the all short-term extremes method, the long-term CDF of the short-term extreme response can also be obtained by the average upcrossing rate formulation in association with the Poisson estimation [1]. The basic assumption for this method is that upcrossings of high response levels are statistically independent, and finally the same expression is obtained as Eq. (2) [21]. Moreover, it has been found that the approximate formulation (1) tends to underestimate the long-term extreme response compared to the exact formulation (2) [5, 22]. In this work, assume that the differences between Eqs. (1) and (2) are not significant in the following study, and the most commonly used formulation (1) is applied for the subsequent derivations.

The N-year extreme response, i.e., the response with a return period of N years, y_N is obtained as:

$$y_N = F_Y^{-1}(1 - P_f) \tag{3}$$

where P_f is the corresponding failure probability for the N-year return period.

It is seen from Eq. (1) that the determination of the extreme response distribution $F_Y(y)$ should be evaluated numerically. The computational effort can be reduced by applying the FORM in connection with the structural reliability analysis. In the following study, the complementary probability distribution (i.e., the exceedance probability) should be applied, which is written as:

$$Q_Y(y) = 1 - F_Y(y) \tag{4}$$

Within the FORM terminology, assume that we would like to estimate the exceedance probability for a given high threshold, y_c and the failure function (i.e., the limit state function) is given as:

$$G(y_c, \mathbf{S}) = y_c - Y \tag{5}$$

and then

$$Q_Y(y_c) = \int_{G(y_c,\mathbf{S})\le 0} F_{\tilde{Y}|\mathbf{S}}(y|\mathbf{s}) f_{\mathbf{S}}(\mathbf{s}) d\mathbf{s} \tag{6}$$

In order to alleviate the calculation of the integral in Eq. (6), the physical variables in the integral are usually transformed into a space consisting of independent and standard normal variables (i.e., the U space). Such a transformation is generally performed by the Rosenblatt transformation [23]:

$$\begin{aligned} U_1 &= \Phi^{-1}(F_{S_1}(s_1)) \\ U_2 &= \Phi^{-1}(F_{S_2|S_1}(s_2|s_1)) \\ &\vdots \\ U_{n+1} &= \Phi^{-1}(F_{\tilde{Y}|S_1,S_2,\cdots,S_n}(y|s_1,s_2,\cdots,s_n)) = \Phi^{-1}(F_{\tilde{Y}|\mathbf{S}}(y|\mathbf{s})) \end{aligned} \tag{7}$$

where Φ denotes the CDF of the standard normal function and F represents the cumulative distribution function of the original random variables. In the transformed U space, the exceedance probability (6) is written as:

$$Q_Y(y_c) = \int_{G_{\mathbf{U}}(\mathbf{u})\le 0} \phi_{\mathbf{U}}(\mathbf{u}) d\mathbf{u} \tag{8}$$

where the vector $\mathbf{U}=(U_1, U_2, \ldots, U_{n+1})^{\mathrm{T}}$, $G_{\boldsymbol{U}}$ represents the failure function (5) transformed in the U space, and $\phi_{\boldsymbol{U}}$ denotes the standard multivariate normal PDF.

The basic idea behind the FORM for the approximation of the failure probability is that the

failure surface is replaced with an *n*-dimensional hyperplane at the design point, which corresponds to the closest distance to the origin on the failure surface. The principle of the failure probability approximated by the FORM is illustrated in Fig. 1. The closest distance to the origin is given as:

$$\beta = \sqrt{\sum_{i=1}^{n+1} \hat{u}_i^2} \tag{9}$$

where $(\hat{u}_1, \hat{u}_2, \cdots, \hat{u}_{n+1})$ represents the design point, and then the failure probability in Eq. (6) is approximated as:

$$Q_Y(y_c) \approx 1 - \Phi(\beta) \tag{10}$$

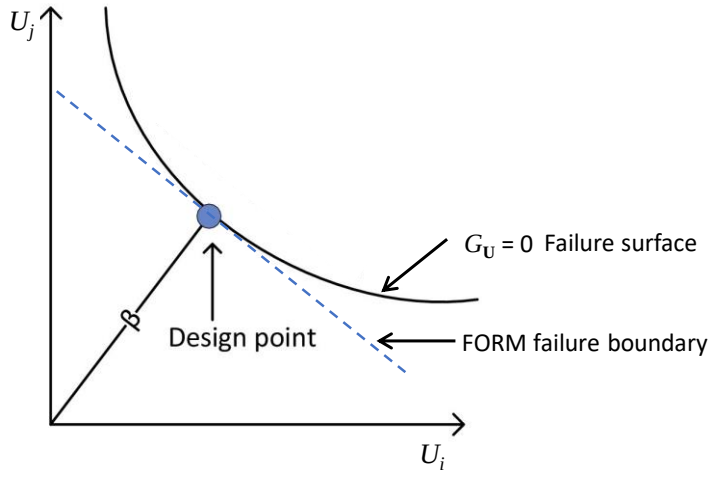

Figure 1. Illustration of the failure probability approximated by FORM in the U space

It is seen in Fig.1 that FORM is a simplified method to calculate the exceedance probability for a given high response level y_c. Different y_c values correspond to different failure surfaces and β values, and therefore, the desired *N*-year extreme response corresponds to a certain exceedance probability, relevant iteration or interpolate schemes that should be applied.

In addition to the abovementioned FORM in association with iteration schemes, the IFORM can also provide a very efficient way to obtain the long-term extreme response that corresponds a given return period. The main idea of the IFORM is that we first specify the exceedance probability and seek the corresponding extreme response level. Therefore, iteration schemes are not required in this method. For a given exceedance probability P_f, the corresponding reliability index is given as $\Phi^{-1}(1- P_f)$. Then, a sphere with the radius $\Phi^{-1}(1- P_f)$ is created in the U space and the target extreme response must be somewhere on the sphere. By transforming the sphere

in the U space into a physical parameter space, the target response level, y_N, is found as the highest value on the surface in the physical parameter space [24, 25].

The main principle of the IFORM is presented as follows: first, an (n+1)-dimensional sphere with the radius $\Phi^{-1}(1- P_f)$ is created in the U space, i.e.:

$$\sum_{i=1}^{n+1} u_i^2 = (\Phi^{-1}(1-P_f))^2 \tag{11}$$

where u_i represents the values of the standard normal variables on the sphere.

Then, transform the variables in the U space into the physical parameter space. According to the last equation in Eq. (7), we obtain:

$$\Phi(u_{n+1}) = F_{\tilde{Y}|\mathbf{S}}(y|\mathbf{s}) \tag{12}$$

and therefore,

$$y = F_{\tilde{Y}|\mathbf{S}}^{-1}(\Phi(u_{n+1})|\mathbf{s}) \tag{13}$$

where the vector $\mathbf{s}=(s_1, s_2, \ldots, s_n)^T$ in the physical parameter space represents the transformed values of the vector $(u_1, u_2, \ldots, u_n)^T$ in the U space, which implies the requirement given by Eq. (11). The maximum value of y in the formulation (13) is selected as an approximation of the target N-year extreme response y_N defined in Eq. (3). In addition, more details on the numerical solution to the IFORM problem, can be found in Refs. [26, 27].

3. Definitions of environmental contours

3.1 ECM and environmental contours based on the IFORM

The development of the ECM for approximating the long-term extreme response prediction is based on the abovementioned IFORM. To begin with, we assume that the variability of the τ-hours short-term extreme response $F_{\tilde{Y}|\mathbf{S}}(y|\boldsymbol{s})$ is not important and can be neglected for estimating the failure probability. Therefore, the random variable U_{n+1} can be set as a fixed value of 0 in Eqs. (11)-(13), and then all combinations of the environmental parameters involved in Eq. (11) can be described by a new (n-dimensional) sphere with radius β_F, i.e.:

$$\sum_{i=1}^{n} u_{i,ECM}^2 = \beta_F^2 \tag{14}$$

where $\beta_F = \Phi^{-1}(1-P_f)$.

When the n-dimensional sphere in the U space, described by Eq. (14), is transformed into

the physical parameter space by the inverse Rosenblatt transformation, the environmental contour that corresponds to the *N*-year return period can be obtained. Since the randomness of the variable U_{n+1} is assumed to be neglected, the median values of the short-term extremes along the abovementioned environmental contour are calculated. The maximum value of these median values [25], given by Eq. (15), would be a good approximation of the long-term extreme response that corresponds to an exceedance probability P_f.

$$y_{ECM} = \max\left\{F_{\tilde{Y}|\mathbf{S}}^{-1}(\Phi(0)|\mathbf{s}_{ECM})\right\} \tag{15}$$

where the vector $\boldsymbol{s}_{ECM}$ represents the short-term environmental conditions on the environmental contour that corresponds to the *N*-year return period.

In reality, for many structures and systems, the variability of the short-term extreme response is important, i.e., the variable U_{n+1} cannot be set as 0 in the U space. In order to compensate the omission of the variability for the short-term extreme response, an empirical fractile value, α, higher than 0.5 is applied to the largest short-term extreme response [24]. Then we obtain:

$$y_{ECM} = \bar{F}_{\tilde{Y}|\mathbf{S}}^{-1}(\alpha|\mathbf{s}_{ECM}) \tag{16}$$

where $\bar{F}_{\tilde{Y}|\mathbf{S}}(\alpha|\boldsymbol{s}_{ECM})$ represents the CDF of the largest short-term extreme response for the environmental conditions on the environmental contour. The fractile value α is structure-dependent, and relevant recommendations for this value can be found in Refs. [8, 24].

It is seen that the ECM is a further simplified method based on the IFORM described in section 2 since there is a one-dimension reduction for the long-term extreme response prediction. In reality, this approximation method has been widely used in the early design stage due to its high efficiency and acceptable accuracy. In this method, a limited set of design conditions is selected on the environmental contour, e.g., see Fig. 2, and then, time consuming calculations for structural responses are only needed for these selected environmental conditions. The main advantage of the ECM used for structural design lies in the fact that the description of the environmental parameters is uncoupled from the structural response and therefore, estimating the long-term extreme response for a given return period can be significantly simplified by determining the environmental contour that corresponds to the same return period.

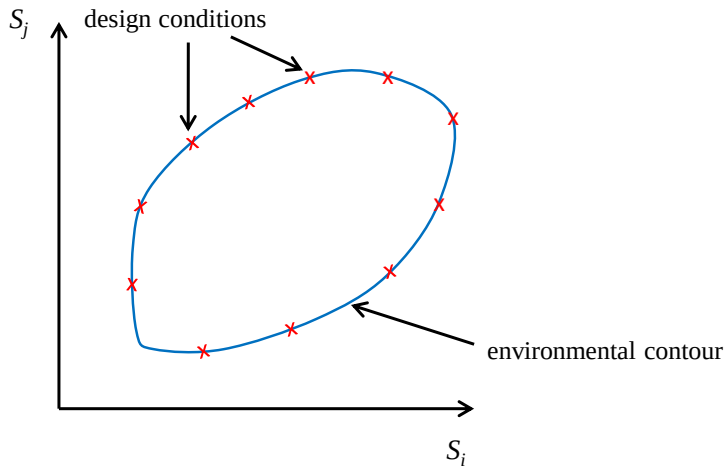

Figure 2. Environmental contour in the physical parameter space and selected environment design conditions

In fact, transforming the sphere with radius β_F in the U space, described by Eq. (14), is the traditional IFORM to generate the environmental contour that corresponds to the N-year return period. The use of the IFORM is a standard design practice for generating environmental contours [8]. In addition, there are also different methods and concepts for the establishment of the environmental contour that corresponds to a given return period, such as the ISORM, the highest density function method [20], direct Monte Carlo simulations [17] and the principal component analysis approach [18].

3.2 Environmental contours based on ISORM

In this section, the principle of the environmental contours based on the inverse SORM (ISORM) is described. Before generation of the ISORM contour, the SORM used for estimation of the failure probability is briefly described. Unlike the FORM approximating the failure surface by a linear function at the design point in the U space, the SORM approximates the failure function $G_{\mathbf{U}}$ (given in Eq. 8) as a quadratic function at the same design point. This second-order failure boundary in the U space can be expressed as:

$$G_{\mathbf{U}\_SORM}(\mathbf{u}) = \sum_{i=1}^{m} a_i (u_i - \delta_i)^2 + \sum_{i=m+1}^{n+1} b_i u_i - c \tag{17}$$

where $G_{\mathbf{U}\_SORM}$ represents the quadratic failure boundary in which (n+1-m) variables occur in linear terms only. In addition, a_i, b_i, δ_i (i=1, 2, …, n+1) and c represent relevant coefficients in the quadratic failure function.

Then, we look back to the failure probability approximation by the FORM in the U space. It is seen in Fig. 3a that, for the convex failure surface in the U space, the FORM approximation gives an upper boundary, and thus overestimates the true failure probability. However, if the true failure region in the U space is a convex set (e.g., view from the origin in Fig. 3b) the FORM approximation underestimates the failure probability. In reality, the shape of the failure surface might be unknown beforehand, and it becomes apparent only during the design process. That means, if the failure surface in the U space is a concave set, the generated environmental contour by the IFORM would be non-conservative for the design purpose [20].

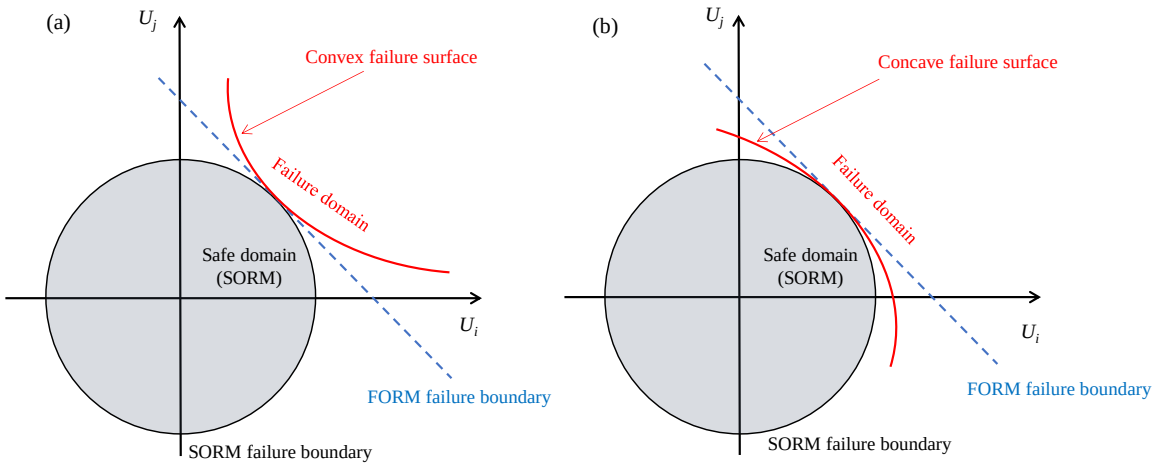

Figure 3. Illustrations of failure probabilities approximated by the FORM and proposed SORM in the U space

In this work, a more conservative concept of environmental contour is proposed to address such a shortcoming of the traditional IFORM. Instead of replacing the failure surface in the U space with a tangent plane at the design point, a sphere with a radius equal to the distance between the origin point and the design point is applied to approximate the failure surface. Then, the complement of the failure domain, i.e., the true safe domain is approximated as the region covered by the sphere. In fact, the proposed sphere in the U space, is a specific kind of second-order failure boundary described by Eq. 17. In this case, the SORM failure boundary corresponds to the quadratic failure function with $a_i = 1$, $b_i = 0$, $\delta_i = 0$ and $c = \beta^2$. It is seen in Fig. 3 that the true failure probability is always overestimated by the proposed (specific) SORM regardless of the shape of the failure surface, since the real safe domain is always larger than the safe domain estimated by the SORM (given as the gray regions). In the specific SORM, the failure probability in Eq. (6) is approximated as:

$$Q_Y(y_c) \approx \int_{\sum_{i=1}^{n+1} u_i^2 \geq \beta^2} \phi_{\mathbf{U}}(\mathbf{u}) d\mathbf{u} \tag{18}$$

Similar to the IFORM, determining the environmental contour for a given return period by the ISORM is also an inverse problem of estimating the failure probability. That means, assume the failure probability P_f is given, then we find the restrictions that impose on the environmental parameters. For establishment of the environmental contour for a given return period by the ISORM, an *n*-dimensional sphere with the radius β_S is created at first. The value of β_S is determined by the following equation:

$$1 - P_f = \int_{\sum_{i=1}^{n} u_i^2 \leq \beta_s^2} \phi_{\mathbf{U}}(\mathbf{u}) d\mathbf{u} \tag{19}$$

For the standard normal variables in the U space, $\sum_{i=1}^{n} u_i^2$ has a χ^2 distribution with *n* degrees of freedom. As a result, the radius βs is expressed as:

$$\chi_n^2(\beta_s^2) = 1 - P_f \tag{20}$$

. Then β_S can be obtained by the inverse function of the χ_n^2 distribution.

It is seen that the corresponding environmental contours obtained by the ISORM for a given return period can always be conservative for the design purpose compared to the environmental contour generated by the traditional IFORM. The sphere is the simplest second-order surface to approximate the failure surface shown in Fig. 3 if we have no more information about the failure surface. Because the principle curvature on the sphere are kept as a fixed value, the solution of environmental contour can be simplified as a one-dimensional problem by taking advantage of the chi-square function shown in Eq. 20. Furthermore, it should be mentioned that, for the proposed ISORM contour, the main drawback is that it tends to give even more conservative results than the IFORM contour if the true failure set is convex.

After creation of the *n*-dimensional sphere with the radius β_F or β_S in the U space, the environmental contour is generated by transforming the independent standard normal variables into physical variables via the inverse Rosenblatt transformation. It is seen that for the environmental contours created by the IFORM or the proposed ISORM, the inverse Rosenblatt transformations are applied since the probabilistic distributions of the environmental variables are described by the conditional modeling approach. However, such a conditional modeling approach requires a great amount of data to establish the conditional distributions between the environmental variables. For the cases where only the marginal PDFs of the environmental variables and the correlation coefficients between the variables are known, the Nataf

transformation can capture these correlations [16]. Then, the environmental contours can be established by applying the Nataf transformation with the abovementioned available data.

In addition to the environmental contour based on the abovementioned ISORM, there is another concept of the "conservative" environmental contour, namely, the highest density contour (HDC) [20]. In this concept, the environmental contour is defined as the boundary of a region that encloses a probability of 1-P_f in the physical parameter space and the joint PDF of the environment parameters $f_{\mathbf{S}}(\mathbf{s})$ is a constant value on the boundary. That means, we have to find a specific boundary with a constant PDF value f_h in the physical parameter space and the region enclosed by this specific boundary is described as:

$$R(f_h) = \{ f_{\mathbf{S}}(\mathbf{s}) \geq f_h \} \tag{21}$$

then, the probability enclosed in the region R is 1-P_f, i.e.:

$$1 - P_f = \int_{R(f_h)} f_{\mathbf{S}}(\mathbf{s}) d\mathbf{s} \tag{22}$$

. Finally, the boundary of the region R, is referred to as the HDC.

Generally, in order to find the specific boundary with a constant joint PDF value of the environmental parameters, the physical parameter space is discretized into a finite number of grid cells (see Fig. 4b) and the value of the joint PDF in each cell is evaluated by numerical integrations. Then, a relevant iteration scheme is applied to find the HDC, i.e., the desired boundary, and the associated region R, within which the enclosed probability is 1-P_f [20]. However, it is seen that the HDC is based on the cell-mapping method, and the computational burden would dramatically increase with the dimensionality of the physical space. Furthermore, for the traditional IFORM-contour and the proposed ISORM-contour in this work, the computation cost is very efficient and nearly independent of the dimensionality of the environmental variables since the solution to the environmental contour reduces to a one-dimensional problem due to the Rosenblatt transformation and rational symmetry of the standard normal distribution.

In fact, the environmental contour obtained by the ISORM is a similar concept to the HDC. In the ISORM, an n-dimensional sphere is created in the U space, and the radius of the sphere β_S is determined in order to fulfill the requirement that the probability enclosed by the sphere is 1-P_f. Since the environmental contour in the physical parameter space is obtained by the inverse Rosenblatt transformation, the constant PDF value on the environmental contour could not be preserved. The difference between the ISORM-contour and the HDC concept is shown in Fig. 4.

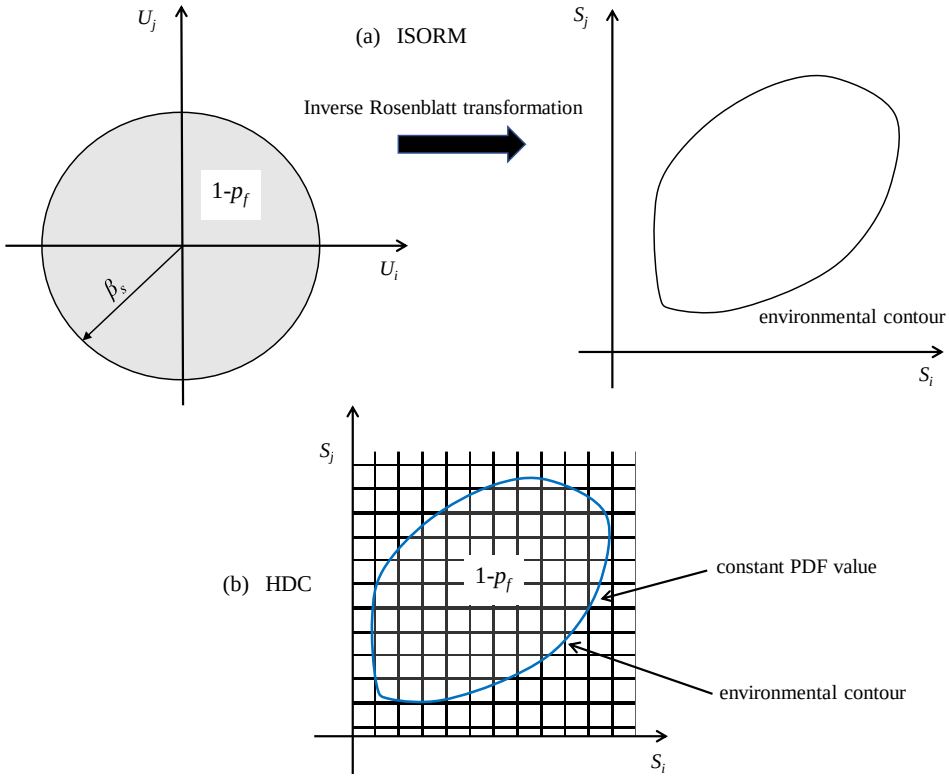

Figure 4. Illustrations of the environmental contour generated by the ISORM and the concept of HDC

4. Applications and comparisons

4.1 Wave statistics

In this section, the wave statistics described by the significant wave height H_s and the wave period T_z (zero up-crossing period) are selected for study. The joint distribution of H_s and T_z is obtained by the conditional modeling approach described and applied in Refs. [8, 28]. This probabilistic model consists of a marginal PDF for the significant wave height and a conditional PDF for the wave period, which is given as

$$f_{H_s T_z}(h_s, t_z) = f_{H_s}(h_s)\, f_{T_z|H_s}(t_z \,|\, h_s) \tag{23}$$

The marginal PDF of H_s is described by a three-parameter Weibull distribution:

$$f_{H_s}(h_s) = \frac{\beta_{H_s}}{\alpha_{H_s}}\left(\frac{h_s - \gamma_{H_s}}{\alpha_{H_s}}\right)^{\beta_{Hs}-1} \exp\left\{-\left(\frac{h_s - \gamma_{H_s}}{\alpha_{H_s}}\right)^{\beta_{Hs}}\right\} \tag{24}$$

where α_{H_s} and β_{H_s} are the scale and shape parameters for the Weibull distribution, respectively. γ_{H_s} is the location parameter of the distribution.

For the conditional distribution of the wave period with a given significant wave height, it is modelled by a lognormal distribution:

$$f_{T_z|H_s}(t_z|h_s) = \frac{1}{\sqrt{2\pi}\sigma_{\ln T_z} t_z} \exp\left\{-\frac{(\ln(t_z) - \mu_{\ln T_z})^2}{2\sigma^2_{\ln T_z}}\right\} \tag{25}$$

in which the mean value μ_{lnT_z} and standard deviation σ_{lnT_z} of $\ln(T_z)$ are assumed to be dependent on the significant wave height in the following manner:

$$\begin{aligned} \mu_{\ln T_z} &= E[\ln(T_z)] = a_1 + a_2 h_s^{a_3} \\ \sigma^2_{\ln T_z} &= Var[\ln(T_z)] = b_1 + b_2 \exp(b_3 h_s) \end{aligned} \tag{26}$$

In this work, the wave statistics were sampled every 6th hour in the North Atlantic Ocean from January 1958 to February 2002 [29, 30]. The parameters for the three-parameter Weibull distribution described by Eq. (24) are obtained by a least squares fit and these values are given as: α_{H_S}= 2.776, β_{H_S}= 1.471, γ_{H_S}= 0.889. The coefficients a_i and b_i (i=1, 2, 3) in Eq. (26) are estimated from actual data and these coefficients are obtained as: a_1 = 0.100, a_2 = 1.489, a_3 = 0.190, b_1 = 0.040, b_2 = 0.175 and b_3 = -0.224 [29].

For different return periods, the corresponding failure probabilities, P_f, are given in Table 1. The radiuses of the cycles in the U space, i.e., β_F and β_S are also shown in this Table. Since the ISORM has a more conservative restriction on the environmental variables, the value of β_S is always larger than that of β_F for the same return period. This difference in the U space is further illustrated in Fig. 5, in which the left figure shows the principle of the traditional IFORM with P_f = 1-Φ(β_F) and the right figure presents the principle of the proposed ISORM with $\chi^2_2(\beta_S^2) = 1 - P_f$.

Table 1. Different return periods and the corresponding failure probabilities, P_f =1/(N·365.25·24/τ), the radiuses of the cycles in the IFORM, β_F, and in the ISORM, β_S

Return period	P_f	β_F	β_S
10 years	6.845E-05	3.814	4.379
25 years	2.738E-05	4.034	4.584
50 years	1.369E-05	4.194	4.733
100 years	6.845E-06	4.349	4.877

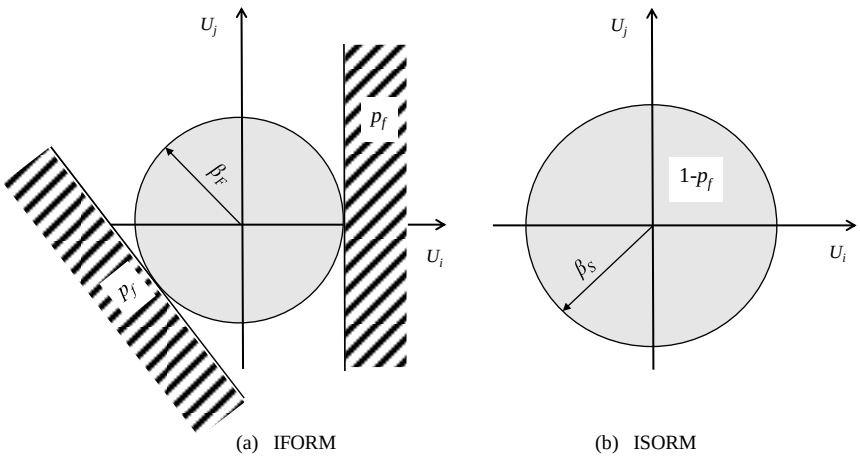

Figure 5. Differences between the IFORM and the ISORM used to generate the environmental contour for a given period in the U space

By applying the inverse Rosenblatt transformation, the environmental contours based on the IFORM and the ISORM for different return periods can be obtained. As an example, the 25-year contours generated by the IFORM and the ISORM are shown in Fig. 6. In addition, a total of 36525 sea state points (i.e., 25 years of 6-h samples) reproduced by Monte Carlo simulation is also plotted in Fig. 6 as a 25-year data set. It is seen in Fig. 6 that the environmental contours generated by the ISORM and the IFORM have the similar shapes, but the ISORM-contour covers a larger area than the IFORM-contour for the same return period since the latter has more conservative restrictions on the environmental variables.

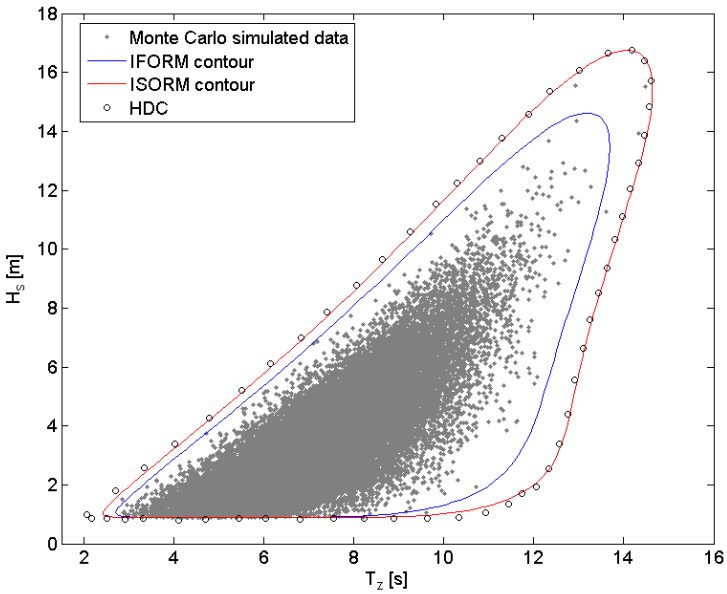

Figure 6. The 25-year environmental contours obtained by the IFORM and the ISORM, the HDC for the same return period, and sea states generated by Monte Caro simulation

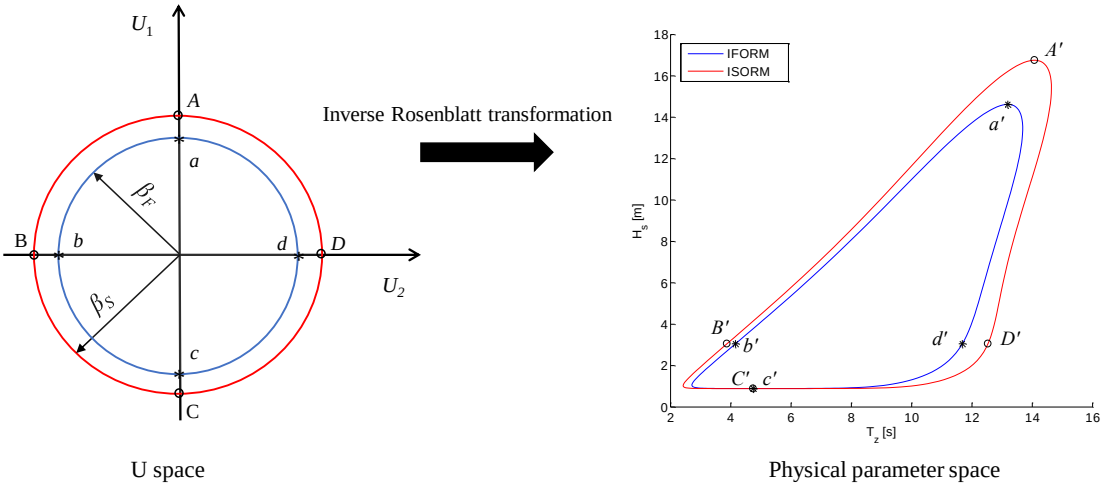

Figure 7. Illustration of the inverse Rosenblatt transformation and the difference between the environmental contours generated by the IFORM and the ISORM for the same return period in the physical parameter space

In order to have a detailed study for the difference between the IFORM-contour and the ISORM-contour for the same return period, the intersection points between the axis in the U space and the cycles with radiuses of β_F and β_S are selected. These points are denoted *a*, *b*, *c* and *d* (for the cycle with the radius β_F), and *A*, *B*, *C* and *D* for the other cycle. The inverse Rosenblatt transformation is illustrated in Fig. 7, and the eight points *a*, *b*, *c*, *d*, *A*, *B*, *C* and *D* are mapped to the corresponding points denoted *a*′, *b*′, *c*′, *d*′, *A*′, *B*′, *C*′ and *D*′ in the physical parameter space by applying one-to-one mapping, i.e., the inverse Rosenblatt transformation. It is seen in Fig. 7 that for negative values of u_1 (corresponds to the significant wave height) and negative values of u_2 of the cycles, the difference between the IFORM-contour and the ISORM-contour is limited. However, such a difference becomes apparent for large values of the significant wave height and wave period, e.g., in the region with $u_1 > 0$ and $u_2 > 0$ on the left figure. Moreover, for different return periods, the maximum values of H_S and *Tz* along the N-year environmental contours generated by the IFORM and ISORM are plotted in Figs. 8 and 9, respectively. Since large values of *Hs* and/or wave period *Tz* are usually associated with large wave energy and serious structural response, such a significant difference revealed by Figs. 6-9 in the current study should be considered in the design of ships and offshore structures.

The environmental contour based on the highest density function, i.e., the HDC for the 25-year return period, is shown in Fig. 6 and the maximum values of H_S and Tz along the *N*-year HDC obtained from Ref. [20] are also plotted in Figs. 8 and 9, respectively. The similarity and difference between the HDC and ISORM-contour have been described in section 3.2. The good

agreements between these two contours for the same return period, shown in Figs. 6, 8 and 9, can be used to verify the correctness of the ISORM-contour in this work. Furthermore, the difference between the ISORM-contour and HDC in the left corner of Fig. 6 can be regarded as being caused by the inverse Rosenblatt transformation since such a nonlinear transformation cannot guarantee the constant value of the joint PDF on the environmental contour in the physical parameter space.

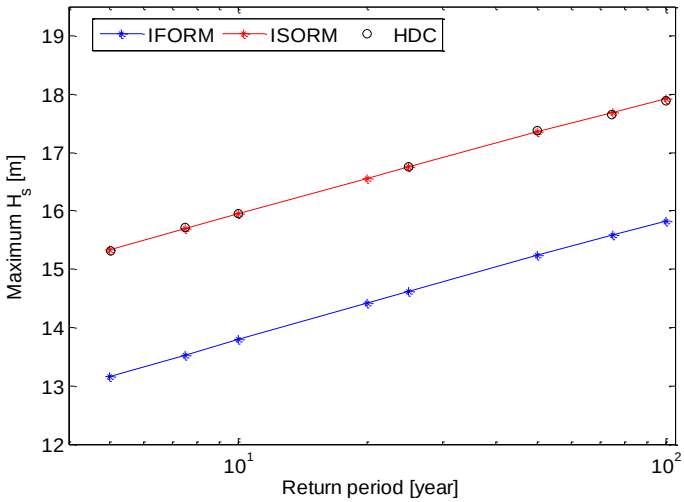

Figure 8. Maximum values of H_S along the environmental contours for different return periods

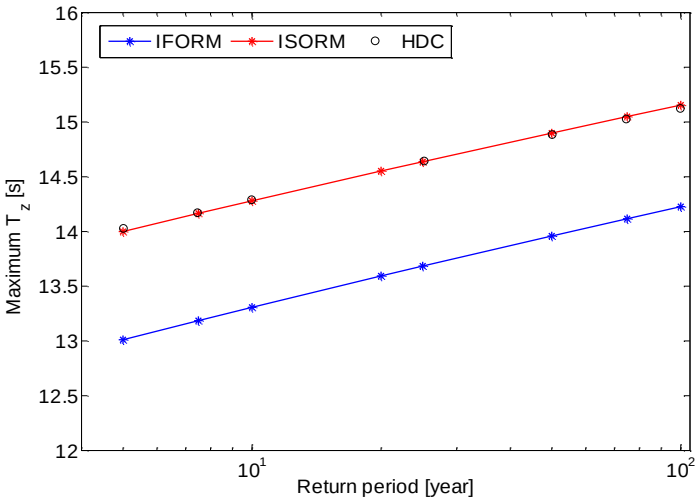

Figure 9. Maximum values of T_z along the environmental contours for different return periods

4.2 Wind and wave statistics

In this section, the wind and sea states in the northern North Sea are considered [31]. The environmental statistics are described by a joint probabilistic model of mean wind speed U_w, significant wave height H_s and spectral peak period T_p, which is given as:

$$f_{U_w H_s T_p}(u_w) = f_{U_w}(u_w) \cdot f_{H_s|U_w}(h_s|u_w) \cdot f_{T_p|H_s U_w}(t_p|h_s u_w) \tag{27}$$

In this joint model, wind is characterized by 1-hour mean wind speed at 10 m above the average sea level and it is assumed to be described by a two-parameter Weibull distribution:

$$f_{U_w}(u_w) = \frac{\beta_{U_w}}{\alpha_{U_w}} \left(u_w/\alpha_{U_w}\right)^{\beta_{U_w}-1} \exp\left(\left(u_w/\alpha_{U_w}\right)^{\beta_{U_w}}\right) \tag{28}$$

where α_{U_w} and β_{U_w} are the scale and shape parameters for the Weibull distribution, respectively. These values were determined to be 1.708 and 8.426 on the basis of the measurements from the northern North Sea in the period of 1973-1999.

The wave statistics were obtained from 3-hour stationary sea states. For the conditional distribution of H_s for a given wind speed U_w, it is suggested to follow a two-parameter Weibull distribution with the scale and shape parameters given as:

$$\alpha_{H_s} = 1.8 + 0.100 \cdot U_w^{1.322} \tag{29}$$

$$\beta_{H_s} = 2.0 + 0.135 \cdot U_w \tag{30}$$

Similar to the probabilistic model given by Eq. (25), the conditional distribution of the spectral peak period T_p for given wind speed U_w and significant wave height H_s is described by a lognormal distribution:

$$f_{T_p}(t_p) = \frac{1}{\sqrt{2\pi}\sigma_{\ln T_p} t_p} \exp\left\{-\frac{(\ln(t_p) - \mu_{\ln T_p})^2}{2\sigma_{\ln T_p}^2}\right\} \tag{31}$$

where μ_{lnT_p} and σ_{lnT_p} are the mean value and standard deviation of $\ln(T_p)$, respectively. They are given by the following equations:

$$\mu_{\ln T_p} = \ln\left(\frac{\mu_{T_p}}{\sqrt{1+\upsilon_{T_p}^2}}\right) \tag{32}$$

$$\sigma_{\ln T_p}^2 = \ln\left(1+\upsilon_{T_p}^2\right) \tag{33}$$

where $v_{T_p} = \sigma_{T_p}/\mu_{T_p}$. The mean value and standard deviation of the spectral peak period T_p are assumed to be dependent on the significant wave height and wind speed by the following two equations:

$$\mu_{T_p} = (4.883 + 2.68h_s^{0.529}) \cdot \left[1 - 0.19\left(\frac{u_w - (1.764 + 3.426h_s^{0.78})}{1.764 + 3.426h_s^{0.78}}\right)\right] \tag{34}$$

$$\sigma_{T_p} = \left[-1.7 \cdot 10^{-3} + 0.259 \cdot \exp\left(-0.113h_s\right)\right] \cdot \mu_{T_p} \tag{35}$$

In this work, the 1-hour mean wind speed is assumed to be representative for a 3-hour stationary condition and then the 50-year environmental contour for the 1-hour mean wind speed versus the 3-hour sea state is considered. This kind of environmental contour can be applied for the design of marine structures, such as offshore wind turbine [13], combined wind and wave energy devices [32]. Since the wind and wave statistics are described by the joint model given in Eq. (27), the inverse Rosenblatt transformation is applied to transform the three-dimensional spheres with radiuses of β_F and β_S in the U space into the desired contour surfaces in the physical parameter space.

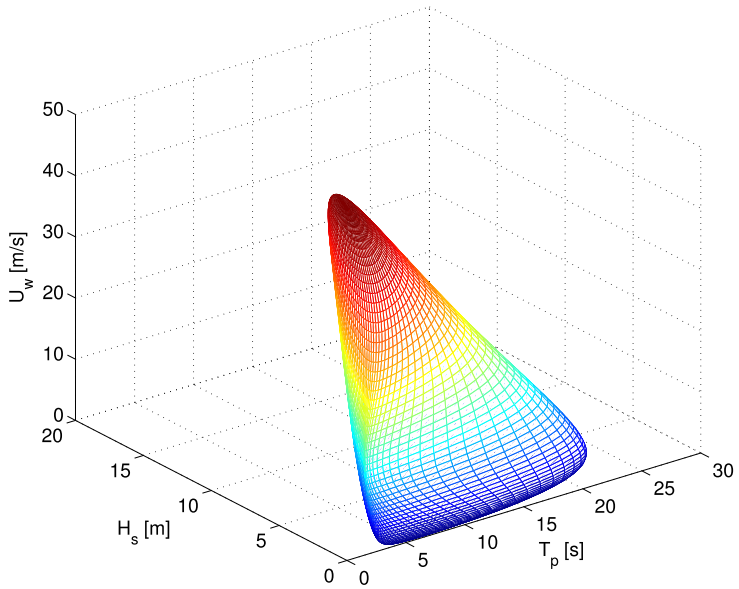

Figure 10. The 50-year contour surface of the joint distribution for mean wind speed and waves generated by the IFORM

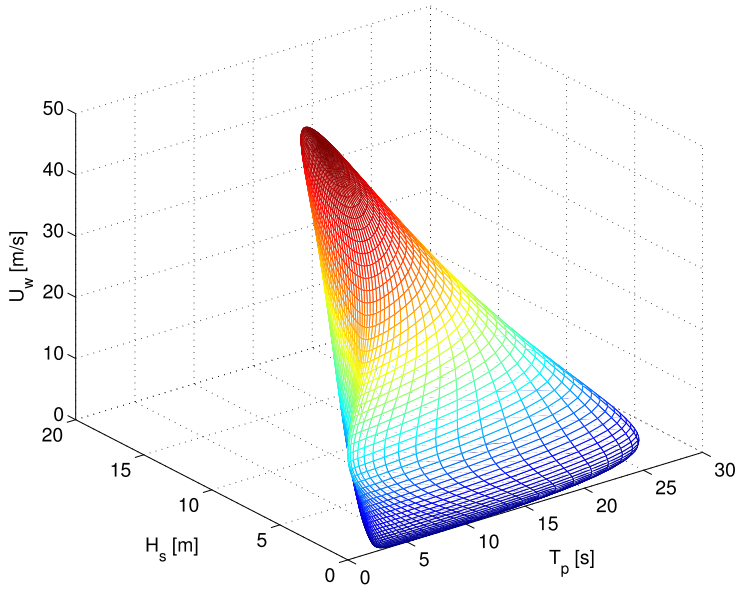

Figure 11. The 50-year contour surface of the joint distribution for mean wind speed and waves generated by the ISORM

The 50-year environmental contour surfaces of the joint distribution for mean wind speed and waves generated by the IFORM and the ISORM are presented in Figs. 10 and 11, respectively. In the U space, the radius of the sphere for the IFORM β_F is equal to 4.349 for the 50 years return period and the corresponding radius for the ISORM β_S is 5.166. It is seen in Figs. 10 and 11 that the contour surfaces generated by the IFORM and ISORM have similar shapes, but the environmental contour obtained by the ISORM method has a wider distribution, since the ISORM-contour has more conservative restrictions on the environmental parameters than the IFORM-contour for the same return period.

In order to have a detailed study of the comparisons between the IFORM-contour and the ISORM-contour for the same return period, two-dimensional contour lines for different wind speeds are considered. The maximum values of the significant wave heights and wave spectral periods along the contour lines for different wind speeds are shown in Fig. 12. Then, taking the NREL (National Renewable Energy Laboratory) 5 MW wind turbine with a reliable floating supporter as an example [33], four representative wind speeds: U_w = 35 m/s (survival model), 25 m/s (cut out wind speed), 11.4 m/s (rated wind speed) and 5 m/s (cut in wind speed), are selected to illustrate the differences of the two-dimensional contour lines obtained by different methods and the results are plotted in Fig. 13.

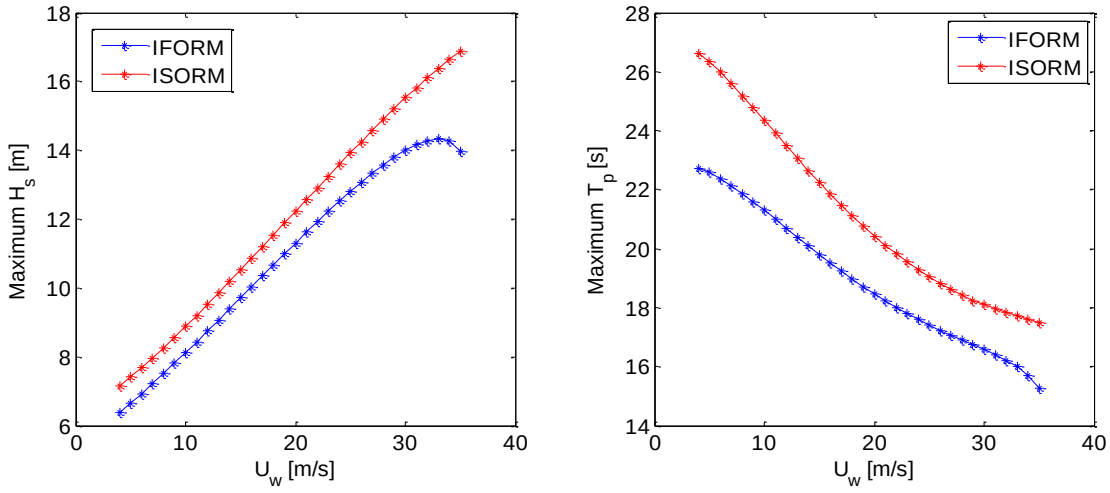

Figure 12. Maximum values of *Hs* and *Tp* of the two-dimensional contour lines for different wind speeds on the 50-year contour surfaces generated by the IFORM and the ISORM

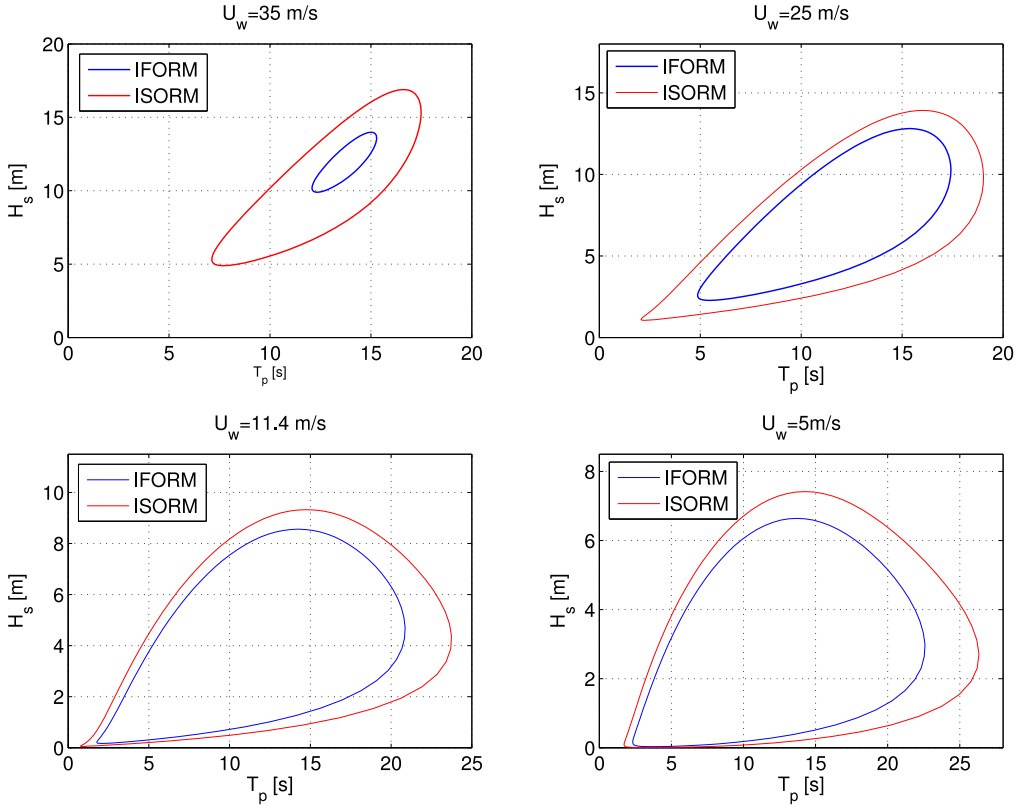

Figure 13. Two-dimensional contour lines for different wind speeds on the 50-year contour surfaces generated by the IFORM and the ISORM

It is seen in Fig. 12 that for a given wind speed, the maximum values of H_s and T_p on the ISORM-contour are always larger than those values on the IFORM-contour. Meanwhile, as observed in Fig. 13, the two-dimensional IFORM-contour lines have similar shapes as the

ISORM-contour lines. Due to more conservative restrictions on the environmental parameters, the ISORM-contour line has a broader range than the IFORM-contour for the same wind speed. Moreover, it is noted in Fig. 13 that for the cut in wind speed and the rated wind speed, the differences between the IFORM-contour lines and the ISORM-contour lines in the regions with small values of *Hs* and *Tp* are not significant and such differences become apparent as increasing values of U_w, *Hs* and *Tp*.

4.3 First-year ice ridge statistics

In recent years, increased plans and activities for maritime transport and for exploiting natural resources, such as oil and gas, minerals, in Arctic regions promoted the requirement of ice-capable vessels and offshore structures [34]. For ships and offshore structures in sea ice fields, a number of different ice types, such as level ice, broken ice, ice ridges (see Fig. 14), will be encountered. Ice ridges are assumed to pose the major threat to the ships and offshore structures in the sea ice area without icebergs, since they determine and govern the design loads for the structures [35].

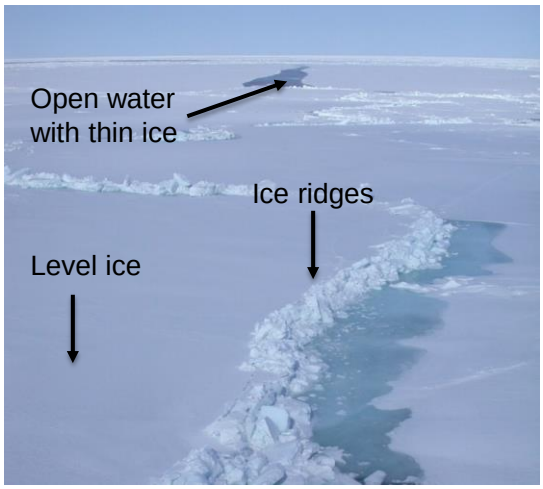

Figure 14. An example of different ice conditions in the Arctic region

A ridge is a line or wall of broken ice features forced up by pressure or shear. More specifically, ice ridges are formed from ice sheets/floes as they break under compression or shear due to wind and current. When first formed, an ice ridge is simply a pile of unconsolidated ice blocks. Then, these blocks may become consolidated to some extent by refreezing processes and form the ice ridge. Fig. 15 illustrates a typical ice ridge, which consists of two parts: the sail and the keel. The sail part is above the water and has pores filled with air and snow. The

keel is the underwater part and can be further separated into an upper completely frozen layer called the consolidated layer, which is always thicker than the surrounding level ice thickness, and a lower unconsolidated part that has loose blocks partially refrozen together with water trapped between the blocks [36].

Basically, ice ridges are divided into the first-year (e.g. Fig. 15), second-year, and multi-year ice ridges. During its first winter and summer, an ice ridge is called a first-year ridge. The consolidation process in the keel part progresses with time and the keel part is close to being fully consolidated if the ridge has survived one summer's melt. The ridges that survive one or more summers are called second-year and multi-year ridges, respectively. In this work, the first-year ridge is considered for the design of ice-capable vessels. For one thing, the ice conditions along the commercial Arctic shipping routes, such as the Northern Sea Route, are mostly first-year and few ice appears in summer seasons. For another, fewer studies have been made on second- and multi-year ice ridges than first-year ice ridges, and information on the physical and mechanical properties is very limited for second- and multi-year ice ridges.

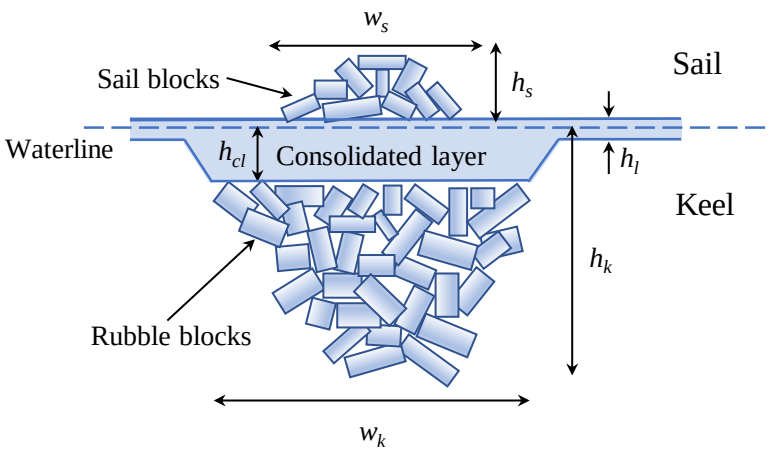

Figure 15. First-year ice ridge with some key parameters: sail draft h_s, sail width w_s, level ice thickness h_l, consolidated layer thickness h_{cl}, keel draft h_k and keel width w_k

In this section, the concept of environmental contours is applied in order to provide an efficient method to estimate the long-term extreme response of ice-capable vessels sailing along the Arctic routes. Since the ice ridges govern the design loads for these ice-capable vessels, the key parameters of the first-year ice ridges that determine the response of a vessel should be identified at first, and then relevant statistical distributions for these key parameters should be applied in order to build the environmental contours for a given return period. In addition, for the ship-ice ridge interaction process with a given set of environmental parameters for the ice

ridge, the variability of the short-term extreme response is assumed not to be important and can be regarded as a fixed value. Then, Eq. (15) is applied to estimate the long-term extreme response by applying the ECM.

For the scenario of an ice-capable ship interacting with a first-year ice ridge, the ship structure can be simplified as a downward sloping structure. The effects of ridge sail for the first-year ice ridge can be neglected since the volume of the sail is small compared to that of the keel part [37]. On the other hand, failure of the consolidated layer is the dominant part in determining the keel loads due to the ice ridge interaction with slope structure. This has been confirmed in Ref. [38] with relevant studies on ice ridges failure against a confederation bridge, whose piers are designed as (slope) ice-breaking cones. In addition, there is no correlation between the keel depth h_k and the keel loads. For the action due to the consolidated layer, it can be approximated as level ice with an equal thickness that interacts with the slope structure and the mechanical properties of the consolidated layer are assumed to be close to those of level ice [35, 37].

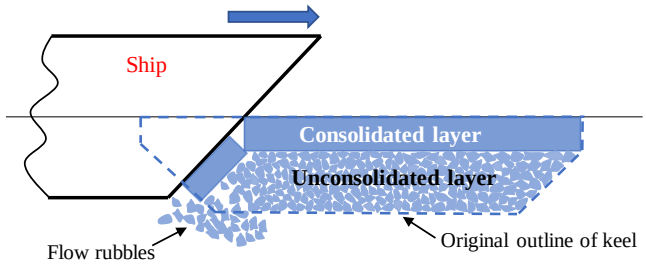

Figure 16. Illustration of a ship interacting with a typical first-year ice ridge

Based on the former studies for first-year ice ridges interacting with slope structures, the ship-ice ridge interaction process is illustrated in Fig. 16. Flow rubbles from the unconsolidated layer would be cleared by the local water current. As a preliminary design, the interaction process can be simplified as a ship-level ice interaction event, which has been studied extensively. Generally, the ship-level ice interaction process is initiated by a localized crushing of the ice edge, and then the contact area between the ship and the ice sheet as well as the crushing force increase with the ship advancing and penetrating the ice features. The ice sheet eventually deflects and the bending stresses promote a flexural failure at a certain breaking distance from the crushing region [39]. Therefore, the thickness, crushing strength and flexural strength of the consolidated layer are considered as the most important parameters for

determining the response of the vessel due to the ship-ice ridge interaction at the early design stage.

In order to build environmental contours used for the design purpose, statistical models should be applied to describe the abovementioned key parameters. The consolidated layer thickness is believed to depend on geographical location and season. In this work, the first-year ice ridges in the Barents Sea are considered, since many field experiments have been performed in this sea area by relevant Norwegian and Russian research institutes. A gamma distribution, Eq. (36), is applied to model the average thicknesses of the consolidated layers, which are collected by mechanical drilling [36]:

$$f(h_{cl}) = \frac{1}{\Gamma(k)\theta^k} h_{cl}^{k-1} \exp(-\frac{h_{cl}}{\theta}) \tag{36}$$

where k and θ are the shape and scale parameters for the gamma distribution, respectively. Based on the experimental data, these two values are determined to be 2.97 and 0.54.

Experimental data for the flexural strength and crushing strength of the consolidated layer are limited and the mechanical properties of the surrounding level sea ice can be applied as an effective alternative [40]. The flexural strength of the level sea ice depends on the average temperature and salinity. On the basis of the experimental data for the flexural strength of the level ice in the Barents Sea in Refs. [41, 42], the marginal PDF of the flexural strength is described by a two-parameter Weibull distribution:

$$f(\sigma_f) = \frac{\beta_{\sigma_f}}{\alpha_{\sigma_f}} \left(\sigma_f / \alpha_{\sigma_f}\right)^{\beta_{\sigma_f}-1} \exp\left(\left(\sigma_f / \alpha_{\sigma_f}\right)^{\beta_{\sigma_f}}\right) \tag{37}$$

where the scale parameter α_{σ_f} = 0.274 and the shape parameter β_{σ_f} = 3.167 are obtained from actual data.

The crushing (or compressive) strength of level sea ice is related to the ice salinity, temperature, density and loading direction [43]. Full-scale measurements have been performed to collect the data of the uniaxial compressive strength of the first-year level ice in the Barents Sea, and the distribution of the crushing strength for the vertically loaded samples can be described by the gamma distribution given in Eq. (36) with a shape parameter of 4.70 and a scale parameter of 0.40 [44]. From the abovementioned measured data obtained by in situ experiments and the probabilistic models given by Eqs. (34) and (35), the probability

distributions of the consolidated layer thickness, flexural strength and crushing strength are presented in Figs. 17, 18 and 19, respectively.

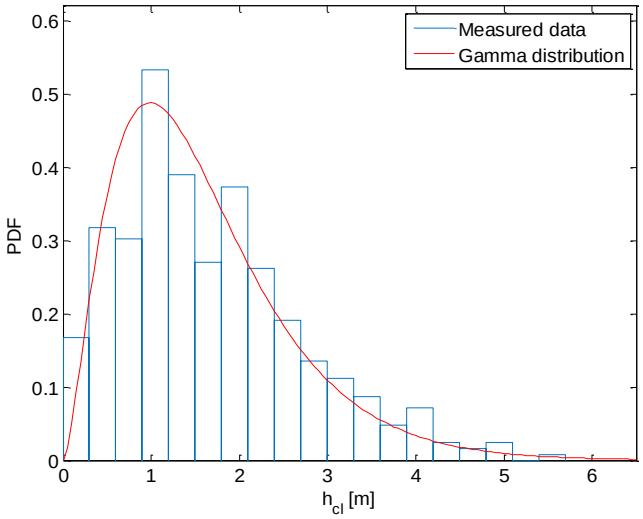

Figure 17. Probability distribution for the consolidated layer thickness h_{cl}

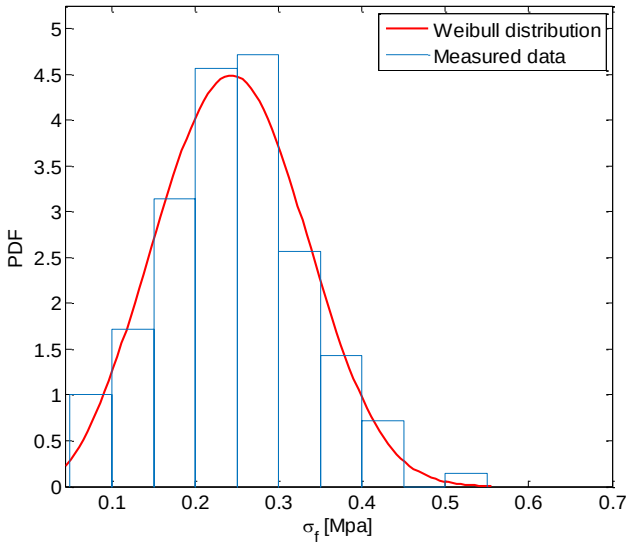

Figure 18. Probability distribution for the flexural strength σ_f

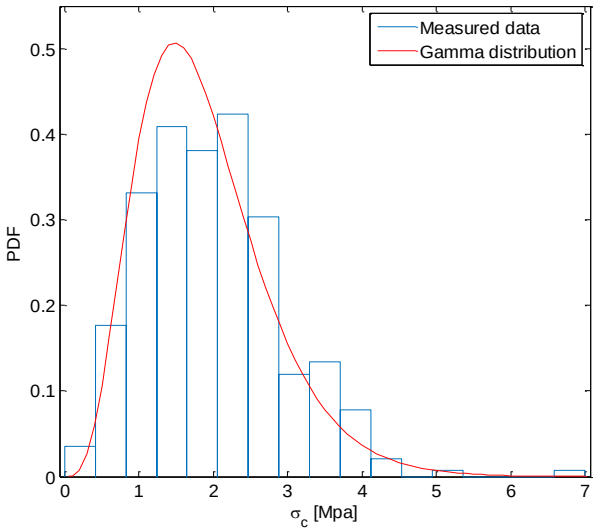

Figure 19. Probability distribution for the crushing strength σ_c

It is seen in sections 3 and 4 that developing the environmental contour requires the joint distribution of the environmental parameters based on the conditional modeling approach. A great amount of sampled data is required to build such a joint distribution for the environmental variables. However, due to the limitation of experimental data for the ice ridge statistics, only the marginal PDFs of the abovementioned key parameters can be obtained. Nevertheless, the joint distribution of the environmental parameters with consideration of the correlations between these environmental variables can be approximated by the Nataf distribution model, and then, the environmental contours can also be obtained by the Nataf transformation [16]. Moreover, it should be noted the Nataf transformation model is essentially a type of copula approach and such simple copula models may fail to describe the data well in some cases [45].

As a simple case for demonstrating the development of environmental contours used for the design of ice-capable vessels, a set of coefficients are introduced for the following study. In this case, the variables S_1, S_2 and S_3 represent the consolidated layer thickness, flexural strength and crushing strength, respectively. The symbols ρ_{12}, ρ_{13} and ρ_{23} represent the correlation coefficients between these variables. Based on the Nataf transformation and the probabilistic distributions of the environmental parameters, the following expressions can be obtained:

$$s_1 = F_{S_1}^{-1}(\Phi(u_1)) \tag{38}$$

$$s_2 = F_{S_2}^{-1}(\Phi(u_2\sqrt{1-\rho_{12}'^2} + \rho_{12}'\Phi^{-1}(F_{S_1}(s_1)))) \tag{39}$$

$$s_3 = F_{S_3}^{-1}(\Phi(\frac{u_3}{\sqrt{1-\rho_{12}'^2}}\sqrt{1-\rho_{12}'^2-\rho_{13}'^2-\rho_{23}'^2+2\rho_{12}'\rho_{13}'\rho_{23}'} + \frac{1}{1-\rho_{12}'^2}((\rho_{13}'-\rho_{12}'\rho_{23}')\Phi^{-1}(F_{S_1}(s_1))+(\rho_{23}'-\rho_{12}'\rho_{13}')\Phi^{-1}(F_{S_2}(s_2))) \tag{40}$$

where U_1, U_2 and U_3 represent independent standard normal variables. The coefficients ρ'_{ij} (i, j =1, 2, 3; $i \neq j$) are the corresponding (equivalent) correlation coefficients used in the Nataf transformation, and their relationships with ρ_{ij} can be approximated by a semi-empirical equation, which is given as:

$$\rho'_{ij} = \zeta \cdot \rho_{ij} \tag{41}$$

Relevant descriptions for determining the function ζ can be found in Ref. [46].

It is seen from Eqs. (38)-(41) that, when a three-dimensional sphere with radius β_F or β_S is created in the U space, the environmental contour for a given return period can be obtained by the IFORM or the ISORM based on the Nataf transformation. Assume that the desired ice-capable ship mainly sails and operates in the Barents Sea with 5000 km of the annual voyage in the ice ridge field and the ice ridge density is 2/km along the route [47]. In addition, the correlation coefficients ρ_{ij} (i, j =1, 2, 3; $i \neq j$) are assumed to be 0.5 in this case study. Therefore, for a 50-year return period, the failure probability is determined by Eq. (42), which is given as:

$$P_f = 1/(50 \cdot 5000 \cdot 2) \tag{42}$$

Correspondingly, the radius of the sphere in the U space used for generating the IFORM contour β_F is determined as 4.611 according to Eq. (14). Similarly, according to Eq. (20), radius β_S = 5.407 is obtained for developing the ISORM-contour for the same return period.

The 50-year contour surfaces generated by the IFORM and the ISORM are plotted in Figs. 20 and 21, respectively. The transformations of the three-dimensional spheres in the U space to the contour surfaces are executed by the Nataf model, in which the statistics of the three key parameters of the first-year ice ridge used for the design of a desired ice-capable vessel are all incorporated. Moreover, in order to present a detailed comparison of these two environmental contours, two-dimensional contour lines for different consolidated layer thicknesses are plotted in Fig. 21. In these four selected consolidated layer thicknesses, h_{cl} = 1.59 m is the mean value of the collected samples.

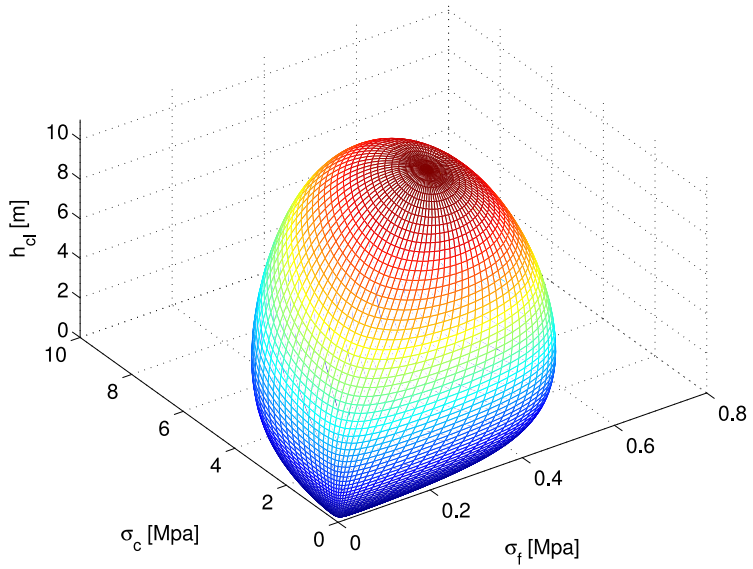

Figure 20. The 50-year contour surface of the consolidated layer thickness, flexural strength and crushing strength generated by the IFORM

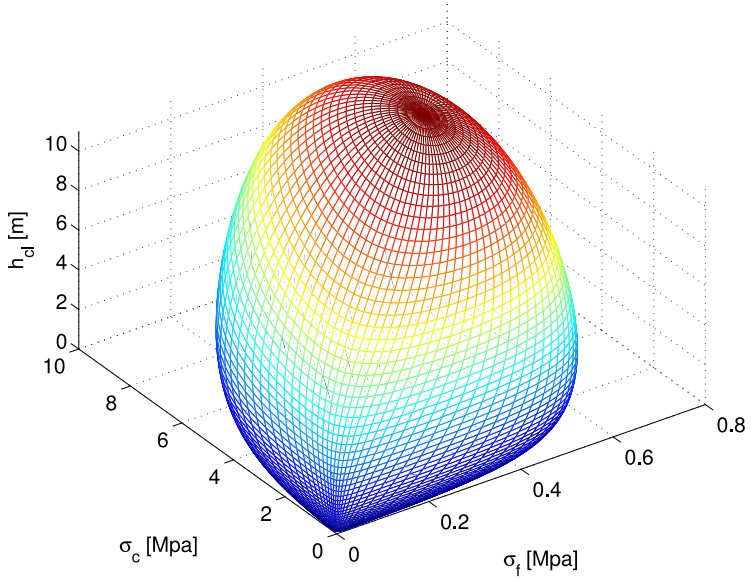

Figure 21. The 50-year contour surface of the consolidated layer thickness, flexural strength and crushing strength generated by the ISORM

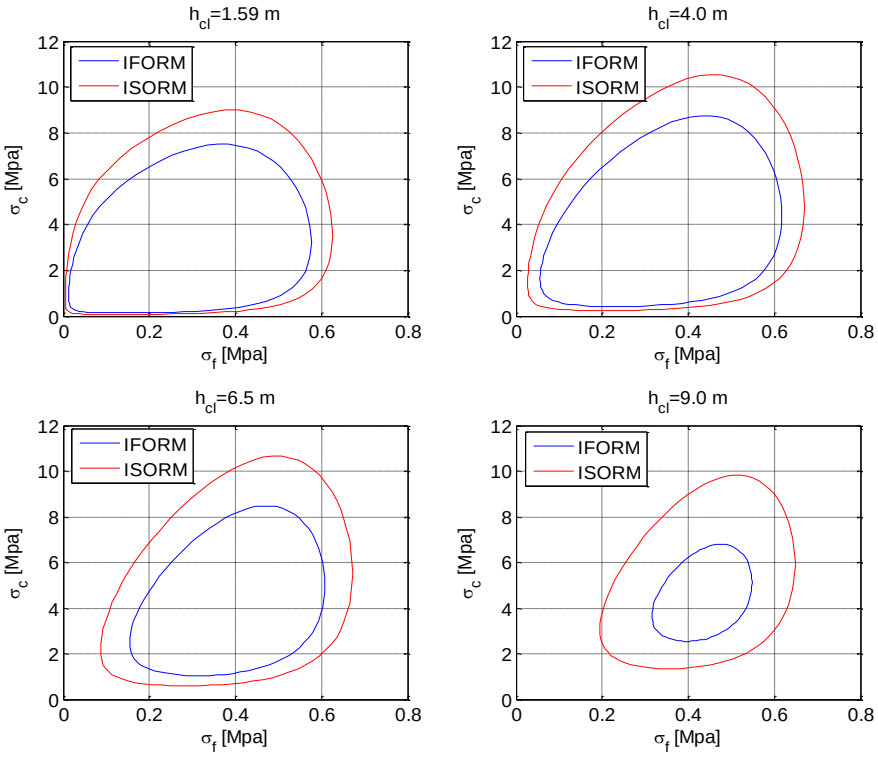

Figure 22. Two-dimensional contour lines for different consolidated layer thicknesses on the 50-year contour surfaces generated by the IFORM and the ISORM

In this case, similar to the examples given in sections 3 and 4, the main difference between the IFORM-contour and the ISORM-contour is that $\beta_F < \beta_S$ due to the different principles behind the IFORM and ISORM for generating environmental contours. It is easily seen in Figs. 20 and 21 that these two contour surfaces have similar shapes and that the ISORM-contour has more conservative restrictions on the three key ice-ridge parameters than the IFORM-contour for the same return period. These findings are consistent with the observations described in section 4. For the noticeable differences between the two-dimensional contour lines shown in Fig. 22, a reliable numerical model is required in order to investigate the difference between the extreme response estimations based on different environmental contours.

Moreover, the correlation coefficients in this simple case are chosen somewhat arbitrarily since there are no former studies for the correlation between these parameters of the sea ice material. Therefore, a relevant study for this could promote the development of the reliability-based design of ships and offshore structures in Arctic regions.

5. Conclusions

In this work, the ECM used for estimating the long-term extreme response in the design of ships and offshore structures was described. The principles behind the traditional IFORM and the proposed ISORM for generating environmental contours to be used in the ECM were presented. Relevant examples, such as the wave statistics, wind wave statistics and first-year ice ridge statistics were applied in order to study the difference between the IFORM-contour and the ISORM-contour.

Based on the abovementioned examples, it is found that the ISORM-contour and the IFORM-contour have similar shapes. However, the ISORM-contour has more conservative restrictions on the environmental parameters than the IFORM-contour, since the former is based on the assumption that the true failure surface of the environmental parameters in the U space is approximated as a specific second-order surface at the design point and the failure domain would be always overestimated regardless of the shape of the failure surface. Therefore, the result of the ISORM-contour is always conservative for the design purpose, which cannot be guaranteed by the traditional IFORM-contour.

Furthermore, noticeable differences between the IFORM-contour and the ISORM-contour for the same return period have been observed in sections 4-6. Therefore, reliable numerical models or experiments are required to study and compare the performance of these two environmental contours used in the ECM for estimating the extreme response of ships and offshore structures at the early design stage. This could be a future work beyond current study.

Acknowledgments

This work has been carried out within the MARTEC research project PRICE (Prediction of ice-ship-interaction for icebreaking vessels) [34]. Financial support from the Research Council of Norway (RCN project number: 249272/O80) are acknowledged. We appreciate the support and valuable comments given by Professor Knut Vilhelm Høyland and PhD candidate Ilija Samardzija during the internal workshop at NTNU. The first author wish to give special thanks to his wife M.B.A Shanhong Yu and parents, Qiwen Chai and Lanxiang Lou for their endless love during the five years overseas study and work in Norway.

References

[1] Naess A, Moan T. Stochastic dynamics of marine structures. Newyork: Cambridge University Press; 2012.

[2] Leira BJ. A comparison of stochastic process models for definition of design contours. Structural Safety. 2008;30:493-505.
[3] Sagrilo L, Næss A, Doria A. On the long-term response of marine structures. Appl Ocean Res. 2011;33:208-14.
[4] Chai W, Naess A, Leira BJ, Bulian G. Efficient Monte Carlo simulation and Grim effective wave model for predicting the extreme response of a vessel rolling in random head seas. Ocean Eng. 2016;123:191-203.
[5] Chai W, Naess A, Leira BJ. Long-term extreme response and reliability of a vessel rolling in random beam seas. Journal of Offshore Mechanics and Arctic Engineering. 2018;140:011601.
[6] Baarholm GS, Moan T. Estimation of nonlinear long-term extremes of hull girder loads in ships. Mar Struct. 2000;13:495-516.
[7] Vanem E. A comparison study on the estimation of extreme structural response from different environmental contour methods. Mar Struct. 2017;56:137-62.
[8] DNV. Recommended practice DNV-RP-C205: Environmental conditions and environmental loads. Norway: Det Norske Veritas 2010.
[9] Winterstein SR, Engebretsen K. Reliability-based prediction of design loads and responses for floating ocean structures. 27th International Conference on Offshore Mechanics and Arctic Engineering, Lisbon, Portugal 1998.
[10] Baarholm GS, Haver S, Økland OD. Combining contours of significant wave height and peak period with platform response distributions for predicting design response. Mar Struct. 2010;23:147-63.
[11] Walter EL, Støle-Hentschel S, Moslet PO. Estimating characteristic load effects on floating structures in ice. ASME 2013 32nd International Conference on Ocean, Offshore and Arctic Engineering: American Society of Mechanical Engineers; 2013. p. V006T07A25-VT07A25.
[12] Muliawan MJ, Gao Z, Moan T. Application of the contour line method for estimating extreme responses in the mooring lines of a two-body floating wave energy converter. Journal of Offshore Mechanics and Arctic Engineering. 2013;135:031301.
[13] Li Q, Gao Z, Moan T. Modified environmental contour method for predicting long-term extreme responses of bottom-fixed offshore wind turbines. Mar Struct. 2016;48:15-32.
[14] Fitzwater L, Cornell CA, Veers PS. Using environmental contours to predict extreme events on wind turbines. Wind Energy Symposium, AIAA/ASME2003. p. 244-58.
[15] Baarholm GS, Haver S. Application of environmental contour lines on a flexible riser. ASME 2010 29th International Conference on Ocean, Offshore and Arctic Engineering: American Society of Mechanical Engineers; 2010. p. 777-84.
[16] Silva-González F, Heredia-Zavoni E, Montes-Iturrizaga R. Development of environmental contours using Nataf distribution model. Ocean Eng. 2013;58:27-34.
[17] Huseby AB, Vanem E, Natvig B. A new approach to environmental contours for ocean engineering applications based on direct Monte Carlo simulations. Ocean Eng. 2013;60:124-35.
[18] Eckert-Gallup AC, Sallaberry CJ, Dallman AR, Neary VS. Application of principal component analysis (PCA) and improved joint probability distributions to the inverse first-order reliability method (I-FORM) for predicting extreme sea states. Ocean Eng. 2016;112:307-19.
[19] Vanem E, Bitner-Gregersen EM. Alternative environmental contours for marine structural design—a comparison study. Journal of Offshore Mechanics and Arctic Engineering. 2015;137:051601.
[20] Haselsteiner AF, Ohlendorf J-H, Wosniok W, Thoben K-D. Deriving environmental contours from highest density regions. Coastal Engineering. 2017;123:42-51.
[21] Naess A. On the long-term statistics of extremes. Appl Ocean Res. 1984;6:227-8.
[22] Giske F-IG, Leira BJ, Øiseth O. Full long-term extreme response analysis of marine structures using inverse FORM. Probab Eng Mech. 2017;50:1-8.
[23] Rosenblatt M. Remarks on a multivariate transformation. The annals of mathematical statistics. 1952;23:470-2.

[24] Haver S, Winterstein SR. Environmental contour lines: A method for estimating long term extremes by a short term analysis. Transactions of the Society of Naval Architects and Marine Engineers. 2009;116:116-27.
[25] Winterstein SR, Ude TC, Cornell CA, Bjerager P, Haver S. Environmental parameters for extreme response: Inverse FORM with omission factors. Proceedings of the ICOSSAR-93, Innsbruck, Austria. 1993:551-7.
[26] Giske F-IG, Leira BJ, Øiseth O. Full long-term extreme response analysis of marine structures using inverse FORM. Probab Eng Mech. 2017.
[27] Li H, Foschi RO. An inverse reliability method and its application. Structural Safety. 1998;20:257-70.
[28] Bitner-Gregersen EM, Cramer EH, Løseth R. Uncertainties of load characteristics and fatigue damage of ship structures. Mar Struct. 1995;8:97-117.
[29] Vanem E, Bitner-Gregersen EM. Stochastic modelling of long-term trends in the wave climate and its potential impact on ship structural loads. Appl Ocean Res. 2012;37:235-48.
[30] Uppala SM, Kållberg P, Simmons A, Andrae U, Bechtold Vd, Fiorino M, et al. The ERA-40 re-analysis. Quarterly Journal of the royal meteorological society. 2005;131:2961-3012.
[31] Johannessen K, Meling TS, Hayer S. Joint distribution for wind and waves in the northern north sea. The Eleventh International Offshore and Polar Engineering Conference: International Society of Offshore and Polar Engineers; 2001.
[32] Wan L. Experimental and Numerical Study of a Combined Offshore Wind and Wave Energy Converter Concept. PhD Thesis, Trondheim, Norway: Norwegian University of Science and Technology; 2016.
[33] Cheng Z, Madsen HA, Chai W, Gao Z, Moan T. A comparison of extreme structural responses and fatigue damage of semi-submersible type floating horizontal and vertical axis wind turbines. Renew Energy. 2017;108:207-19.
[34] Hahn M, Dankowski H, Ehlers S, Erceg S, Rung T, Huisman M, et al. Numerical Prediction of Ship-Ice Interaction: A Project Presentation. ASME 2017 36th International Conference on Ocean, Offshore and Arctic Engineering: American Society of Mechanical Engineers; 2017. p. V008T07A2-VT07A2.
[35] Høyland KV. Ice ridge characteristics and engineering concerns regarding ice ridges. Proc IAHR Int Symp on Ice. Singapore 2014.
[36] Strub-Klein L, Sudom D. A comprehensive analysis of the morphology of first-year sea ice ridges. Cold Regions Science and Technology. 2012;82:94-109.
[37] ISO. 19906: Petroleum and Natural Gas Industries–Arctic offshore structures. Geneva: ISO 2010.
[38] Lemee E, Brown T. Review of ridge failure against the confederation bridge. Cold regions science and technology. 2005;42:1-15.
[39] Jordaan IJ. Mechanics of ice–structure interaction. Engineering Fracture Mechanics. 2001;68:1923-60.
[40] Timco G, Croasdale K, Wright B. An overview of first-year sea ice ridges. PERD/CHC report. 2000:5-112.
[41] Karulina M, Karulin E, Marchenko A. Field investigations of first-year ice mechanical properties in North-West Barents Sea. POAC13-049, Espoo, Finland. 2013.
[42] Krupina NA, Kubyshkin NV. Flexural Strength of Drifting Level First-year Ice in Barents Sea. International Journal of Offshore and Polar Engineering. 2007;17.
[43] Timco G, Weeks W. A review of the engineering properties of sea ice. Cold regions science and technology. 2010;60:107-29.
[44] Strub-Klein L. A Statistical Analysis of First-Year Level Ice Uniaxial Compressive Strength in the Svalbard Area. Journal of Offshore Mechanics and Arctic Engineering. 2017;139:011503.
[45] Vanem E. Joint statistical models for significant wave height and wave period in a changing climate. Mar Struct. 2016;49:180-205.

[46] Liu P-L, Der Kiureghian A. Multivariate distribution models with prescribed marginals and covariances. Probab Eng Mech. 1986;1:105-12.
[47] Martin B, Ove ES, Sören E. A simulation-based probabilistic design method for arctic sea transport systems. Journal of Marine Science and Application. 2016;15:349-69.